PSILOGOS

Research Article

open-access

Compact Diagnostic Geometry of Hippocampal-Output Circuits Across Psychotic and Mood Syndromes: A Reliability-Weighted Topological Analysis

Michael Brown

ABSTRACT

Resting-state studies frequently catalogue significant connections one region at a time, although diagnosis is expressed by the arrangement of abnormalities across several circuits. We asked whether hippocampal-output disturbances form a diagnostically meaningful geometry after the amount and reliability of evidence attached to each pathway are considered. A signed evidence matrix was assembled for seven hippocampal connections evaluated in 475 individuals: 117 with schizophrenia, 103 with bipolar disorder, 96 with major depressive disorder, and 159 healthy participants. Each connection was weighted by the product of its omnibus F statistic and the logarithm of its corrected cluster extent. Weighted signed distances, alteration burden, diagnostic entropy, and seed-level discrimination were calculated. An exact placement test enumerated 6,174 circuit arrangements while preserving each diagnosis's number and direction of alterations. One-pathway deletion and alternative weighting analyses assessed stability. Schizophrenia and bipolar disorder occupied the nearest positions (distance $= 0.329$), whereas bipolar disorder and major depressive disorder were most distant (0.433). Their signed concordance was likewise greatest for schizophrenia and bipolar disorder (0.568). The subiculum carried 54.5% of seed-level discriminatory information, compared with 30.2% for cornu ammonis and 15.4% for dentate gyrus. Total separation was 1.135, below the exact-placement mean of 1.282 ± 0.112, but the departure was not statistically decisive (two-sided $p = 0.2309$). Deleting one pathway changed total separation only from 1.105 to 1.217 (coefficient of variation 3.4%). Hippocampal-output abnormalities encode a stable, compact diagnostic geometry rather than a sharply partitioned set of disorders. The principal organizational feature is a subicular distribution spanning prefrontal, temporal, and motor targets, while the short schizophrenia–bipolar distance arises from concordant anterior cingulate and orbitofrontal reductions. The method distinguishes reliable organization from apparent uniqueness without treating thresholded clusters as independent biomarkers.

Keywords: hippocampus; resting-state functional connectivity; schizophrenia; bipolar disorder; major depressive disorder; signed networks; diagnostic geometry

Program for Recovery and Community Health, Yale School of Medicine, USA
brown.mich524@gmail.com

– **Published:** 5 November 2024

1. INTRODUCTION

Psychiatric diagnosis remains indispensable for clinical communication, treatment selection, and service organization, yet categorical labels only incompletely represent the biological structure of severe mental illness. Schizophrenia, bipolar disorder, and major depressive disorder can differ profoundly in course and immediate management, but they also intersect in cognition, affect regulation, psychomotor function, sleep, and genetic liability. The Research Domain Criteria initiative formalized the need to relate such dimensions to neurobiology rather than assume that every diagnostic boundary marks a separate mechanism.[2,3] Large-scale genetic work subsequently demonstrated extensive pleiotropy among psychiatric disorders,[5,6] while meta-analytic evidence identified convergent immune and cortical abnormalities that cross conventional categories.[4,7] Regional transcriptional heterogeneity across frontal and hippocampal tissue offers a further reason to expect circuit-specific, rather than diagnosis-wide, similarity.[14] These observations do not erase diagnosis. Instead, they make the geometry among diagnoses an empirical question: two categories may be close in one neural system, distant in another, and internally heterogeneous in both.

Resting-state functional magnetic resonance imaging offers a direct way to study this geometry because it estimates coordinated low-frequency activity across distributed regions without imposing a particular cognitive task. Across schizophrenia, bipolar disorder, and major depressive disorder, disturbances have been described in frontal, limbic, striatal, and default-mode systems.[8,10,27] Structural work reaches a related conclusion: group-average abnormalities overlap, yet the magnitude and spatial distribution vary by syndrome.[9,11,12] A persistent analytical difficulty is that whole-brain maps are usually interpreted cluster by cluster. This practice is appropriate for localization, but it offers no formal account of how the full set of altered connections positions diagnoses relative to one another. A list of significant clusters cannot by itself determine whether an apparently distinctive pathway is indispensable, whether several modest connections collectively dominate the pattern, or whether the diagnostic arrangement would be typical after alteration counts are held fixed.

The hippocampus is especially suited to addressing this problem. It is neither a uniform memory structure nor an isolated medial-temporal node. Cornu ammonis, dentate gyrus, and subiculum differ in cytoarchitecture, intrinsic computation, and extrahippocampal projection pattern.[20,21,26] Cornu ammonis supports recurrent association and retrieval, dentate gyrus contributes to pattern separation, and the subiculum provides a major route through which hippocampal activity reaches cortical and subcortical systems. These divisions matter in psychiatric illness. Meta-analysis and multisite studies document hippocampal volume alterations in schizophrenia and bipolar disorder,[13,16,22] and functional studies identify abnormal subfield coupling in schizophrenia and depression.[23,24] The hippocampus also interacts with dopamine-sensitive striatal circuitry, medial frontal control systems, and temporal association cortex, placing it at the intersection of memory, salience, reward, and psychomotor regulation.[15,32,33]

Subdivision, however, creates a second analytical problem. Once several seeds and several cortical targets are tested, attention may be drawn to the strongest individual connection even when a broader output sector carries more diagnostic information. A pathway can have a large omnibus statistic because all patient groups differ similarly from healthy participants; such a connection may be biologically important but contribute little to discrimination among patient groups. Conversely, a moderately weighted pathway can be diagnostically useful when its direction differs across diagnoses. Distinguishing biological burden from diagnostic discrimination therefore requires separate quantities. The former should reflect how much reliable abnormal evidence is present for a group; the latter should increase when the sign pattern varies across groups. Network neuroscience has long emphasized that connections acquire meaning through their position within a larger system,[38,39] but that principle is not automatically respected when corrected clusters are narrated independently.

Another concern is the instability of conclusions based on thresholded functional imaging. Spatial-extent inference can be sensitive to the cluster-forming threshold and smoothness assumptions.[25] Even when corrected findings are accepted, cluster size is not an effect magnitude, and an omnibus F statistic does not disclose a post-hoc direction. A defensible secondary computation must therefore avoid pretending that either quantity is a participant-level effect size. It should use cluster extent and F only as graded evidence weights, retain the observed post-hoc direction separately, and examine whether results survive reasonable alternative weighting rules. Such restraint is particularly important when only published group-level quantities are available. The analytical target is then the organization of reported evidence, not a reconstruction of unobserved time series or individual variation.

The present study develops a signed, reliability-weighted topological method for this purpose. Seven hippocampal-output pathways are represented as a diagnosis-by-connection matrix. Negative, positive, and null post-hoc outcomes define the sign of each cell, while an attenuated product of omnibus strength and cluster extent defines the connection weight. This construction enables four complementary analyses. Weighted distance places the three patient groups in a common circuit space. Signed concordance separates agreement in direction from mere overlap. Diagnostic entropy identifies pathways that discriminate among patient groups, and aggregation by hippocampal seed quantifies which output sector carries that information. Exact enumera-

tion then asks whether the observed spatial assignment of alterations is unusually compact or dispersed after the number and direction of abnormalities in each group are preserved. Finally, pathway deletion and alternative weighting rules determine whether the geometry depends on a single connection or on an arbitrary definition of reliability.

This approach differs from a search for a unique imaging marker. A single diagnostic marker would require independent participant-level validation, prediction in held-out samples, and careful calibration. The present question is narrower and more fundamental: does the arrangement of statistically supported hippocampal-output disturbances contain nontrivial diagnostic structure, and which hippocampal output sector organizes that structure? We anticipated that schizophrenia and bipolar disorder would occupy adjacent positions because both engage psychosis-related frontal and striatal systems, but we did not assume that their proximity would exceed an exact count-preserving expectation. We further expected the subiculum to dominate diagnostic discrimination because it links hippocampal computation to multiple frontal, temporal, and motor territories. Confirmation would support a distributed-output account; failure would indicate that apparently differentiated pathways do not collectively produce a stable geometry. Either outcome is informative because it separates robust organization from a visually compelling list of regional findings.

The resulting analysis is intentionally auditable. Every matrix entry, weight, permutation, and deletion can be regenerated from a short data table and an openly readable script. Numerical conclusions are reported with bounded interpretation: distances describe this circuit evidence set, not symptom-free diagnostic essences; reliability weights order the available clusters, not biological truth; and exact placement tests evaluate pathway assignment conditional on the observed alteration counts. By making these conditions explicit, the study offers a reproducible bridge between mass-univariate neuroimaging findings and system-level psychiatric interpretation.

2. MATERIALS AND METHODS

The analysis corpus was transcribed from the cohort and inferential tables of Song and colleagues.[1] It comprised 475 individuals retained after motion-quality control: 117 with schizophrenia (SZ), 103 with bipolar disorder (BD), 96 with major depressive disorder (MDD), and 159 healthy controls (HC). Participants were 13–45 years old, illness duration was less than five years in the clinical groups, and diagnoses were established with DSM-IV structured interviews. Resting-state images had been acquired at 3 T with 200 volumes, repetition time 2,000 ms, echo time 30 ms, 35 axial slices, 3 mm thickness, and eyes closed. The imaging analysis had used bilateral probabilistic cornu ammonis (CA), dentate gyrus (DG), and subiculum (SUB) seeds, Fisher-transformed seed-to-voxel connectivity, an omnibus analysis of covariance, and corrected post-hoc contrasts against HC. The present computations used only the retained group counts, descriptive clinical quantities, corrected clusters, peak coordinates, omnibus F values, and post-hoc directions. No participant image, time series, or individual clinical record was accessed.

The cohort quantities in Table 1 provide clinical context rather than inputs to the topological distance. Education and head motion differed across groups in the imaging analysis and had therefore been included as covariates together with age and sex. Symptom scales also differed markedly, as expected from diagnostic ascertainment. Incorporating these scale means directly into circuit weights would conflate clinical severity with evidence reliability and would be especially problematic because scale-specific sample sizes varied. We consequently kept clinical description and circuit topology separate.

Seven connections met the corrected omnibus and post-hoc criteria: CA–anterior cingulate cortex (ACC), CA–right caudate, DG–ACC, SUB–left middle temporal gyrus (MTG), SUB–left inferior orbital frontal gyrus (IFOG), SUB–right middle frontal gyrus (MFG), and SUB–supplementary motor area (SMA). A decrease relative to HC was coded -1, an increase was coded $+1$, and the absence of a corrected post-hoc difference was coded 0. The zero code means that the specified corrected comparison was not supported; it does not establish physiological equivalence. Peak Montreal Neurological Institute coordinates localize each target cluster but were not treated as centroid coordinates, because a peak does not describe the complete cluster geometry.

The matrix in Table 2 contains two kinds of information that must remain distinct. The sign triplet describes diagnostic direction, whereas cluster extent and F describe the strength of the omnibus evidence. The MFG connection, for example, contributes substantially to alteration burden because all three clinical groups show the same negative sign, but it contains no sign variation that can separate those groups. The MTG connection has a different role: its positive BD entry supplies diagnostic contrast even though no negative effect is assigned to SZ or MDD.

2.1. Reliability weighting

For connection e, reliability was defined as

$$r_e = F_e \log(1 + c_e), \qquad w_e = \frac{r_e}{\sum_{k=1}^{E} r_k}, \tag{1}$$

where F_e is the omnibus statistic, c_e is corrected cluster extent in voxels, and $E = 7$. The logarithm limits the influence of spatial extent, because cluster size depends on image smoothness and thresholding and cannot be interpreted as a linear effect magnitude. Normalization gives $\sum_e w_e = 1$, allowing distances and burdens to be compared on a common scale. The weight is therefore a

Table 1. Cohort quantities used in the analysis.

Quantity	SZ	BD	MDD	HC
Participants, n	117	103	96	159
Age, years	24.52 (8.95)	25.79 (7.62)	25.33 (9.22)	26.12 (8.05)
Education, years	10.63 (2.87)	12.52 (2.94)	11.99 (2.88)	14.42 (3.30)
Mean framewise displacement	0.12 (0.06)	0.11 (0.05)	0.13 (0.06)	0.11 (0.05)
HAMD-17	7.87 (6.96)	11.92 (9.53)	21.60 (9.64)	1.15 (1.66)
HAMA	6.80 (7.81)	8.41 (8.30)	17.11 (9.68)	0.85 (1.83)
YMRS	2.19 (4.48)	7.69 (9.91)	1.57 (2.95)	0.16 (0.54)
BPRS	35.64 (13.87)	26.27 (9.38)	26.70 (6.83)	18.27 (0.76)
WCST correct responses	18.03 (11.93)	23.81 (12.83)	24.18 (12.15)	29.86 (12.14)

Table 2. Signed hippocampal-output evidence matrix.

Seed	Target	Voxels	x	y	z	F	SZ / BD / MDD
CA	ACC	82	0	24	24	8.1925	$-1/-1/0$
CA	right caudate	77	9	12	-3	7.0620	$-1/0/0$
DG	ACC	68	0	24	24	8.0583	$-1/-1/0$
SUB	left MTG	178	-51	-36	-3	9.0897	$0/+1/0$
SUB	left IFOG	128	-39	27	-6	8.5548	$-1/-1/0$
SUB	right MFG	134	33	39	24	6.7541	$-1/-1/-1$
SUB	SMA	128	3	15	48	6.6360	$0/-1/0$

ranking device for the reported evidence, not an estimate of a population connectivity coefficient. This distinction follows established caution about network construction and spatial inference in functional imaging.[25,40]

Alternative analyses used uniform weights, F alone, and $\log(1+c)$ alone. Agreement across these definitions indicates that the diagnostic ordering is not created by multiplying F and cluster extent. Disagreement would identify a conclusion that depends on an arbitrary evidence scale.

2.2. Signed diagnostic geometry and concordance

Let $s_{ge} \in \{-1, 0, +1\}$ denote the sign for group g and connection e. The reliability-weighted distance between groups g and h was

$$d(g,h) = \frac{1}{2}\sqrt{\sum_{e=1}^{E} w_e (s_{ge} - s_{he})^2}. \tag{2}$$

The factor $1/2$ places the theoretical maximum at one when every connection has opposite signs. A negative-versus-zero difference contributes one quarter as much squared discrepancy as a negative-versus-positive difference. This ordering is appropriate because opposite directions provide stronger diagnostic contrast than a supported direction paired with an unsupported comparison. The three-by-three distance matrix was embedded in two dimensions by classical multidimensional scaling solely for display; all reported distances were calculated in the complete seven-connection space.

Signed concordance quantified identical nonzero directions relative to the reliability mass altered in either member of a pair:

$$C(g,h) = \frac{\sum_e w_e \, \mathbb{I}(s_{ge} = s_{he} \neq 0)}{\sum_e w_e \, \mathbb{I}(|s_{ge}| + |s_{he}| > 0)}. \tag{3}$$

This weighted Jaccard form is zero when no altered connection has the same direction and one when the two signed patterns coincide. It does not reward two zero entries, because joint absence of corrected evidence is not positive evidence of agreement. Alteration burden for group g was computed as $B_g = \sum_e w_e |s_{ge}|$. Burden and concordance answer different questions: the first describes the reliability mass assigned to any alteration, whereas the second describes directional agreement between groups.

2.3. Pathway discrimination and seed attribution

Diagnostic variation on connection e was measured by the entropy of its three signs. If p_{eq} is the proportion of groups with sign category $q \in \{-1, 0, +1\}$, then

$$H_e = -\frac{\sum_q p_{eq} \log p_{eq}}{\log 3}, \qquad D_e = w_e H_e. \tag{4}$$

Entropy equals zero when all groups have the same sign and approaches one as the three sign categories become evenly represented. The discrimination score D_e therefore requires both sign diversity and reliable evidence. Seed-level contribution was the sum of D_e over connections originating in CA, DG, or SUB, divided by the total

across all connections. This attribution does not claim that a larger anatomical seed is intrinsically more important; it states how the available diagnostic information is distributed across the tested output sectors.

2.4. Exact placement experiment

The observed total separation was $T = d(\mathrm{SZ}, \mathrm{BD}) + d(\mathrm{SZ}, \mathrm{MDD}) + d(\mathrm{BD}, \mathrm{MDD})$. An exact conditional test evaluated whether the placement of altered signs across the seven named connections produced unusually compact or dispersed geometry. Each arrangement preserved the marginal sign counts: five negative SZ entries; five negative and one positive BD entry; and one negative MDD entry. Signs were reassigned to connections without replacement within each group, and assignments were independent across groups. Enumeration yielded all 6174 possible arrangements. A two-sided probability was calculated by doubling the smaller conditional tail around the observed T, with a plus-one correction in numerator and denominator. Because every allowed assignment was enumerated, Monte Carlo error is absent.

This experiment controls a critical nuisance property of the evidence matrix. BD has six altered connections, SZ has five, and MDD has one; these unequal counts mechanically affect pairwise distance. The exact distribution asks whether the particular anatomical placement of those counts adds structure beyond the counts themselves. It does not test the validity of the underlying corrected clusters, and it does not generate synthetic participants.

2.5. Deletion and weighting experiments

Dependence on individual pathways was assessed by omitting each of the seven connections in turn, renormalizing the remaining weights, and recalculating all pairwise distances and T. We summarized the minimum, maximum, and coefficient of variation of deletion-specific T. The diagnostic ordering was considered stable when the identity of the nearest and farthest group pairs was retained. In parallel, the four weighting definitions described above were applied to the complete sign matrix. These analyses address complementary forms of fragility: deletion detects domination by a single connection, whereas weight variation detects dependence on the numerical construction of reliability.

All calculations were implemented in Python 3 using NumPy, pandas, SciPy-compatible linear algebra, and Matplotlib. The project archive contains the two comma-separated input tables, analysis script, numerical outputs, and figure-generation code. Values are printed to three decimals in the text, while unrounded quantities are retained in machine-readable output.

2.6. Ethical considerations

No participant-level record or identifiable information was obtained, and no additional contact, intervention, or image processing was performed. The computations operate on published aggregate quantities. The participant study from which those quantities were transcribed had institutional approval and documented consent. Separate approval was therefore not required for this non-identifiable aggregate analysis under common institutional policies; journal and local requirements should nevertheless be confirmed by the submitting authors.

3. RESULTS AND DISCUSSION

3.1. Anatomical distribution of the circuit set

The seven connections span three hippocampal output sectors and six extrahippocampal targets. CA and DG converge on the ACC, while CA additionally couples with the right caudate. SUB reaches a broader set consisting of left IFOG, right MFG, left MTG, and SMA. This distribution places the evidence set across medial and lateral prefrontal control territories, striatum, temporal association cortex, and medial motor cortex. It is therefore anatomically capable of expressing cognitive, affective, reward-related, and psychomotor distinctions without assuming that any one target maps uniquely to a symptom domain.

Figure 1. Anatomical context of hippocampal output.

The anatomical plate in Fig. 1 provides orientation for the medial-temporal origin of the connections and the distributed cortical field in which the target clusters lie. It is not used for localization or measurement; the numerical localization is defined by the MNI peaks in Table 2. This separation between orientation and quantification prevents a realistic rendering from being mistaken for a statistical parametric map.

The broad SUB target distribution is consistent with its role as a principal hippocampal efferent structure.[26] The subiculum integrates CA1 output and communicates with frontal, temporal, diencephalic, and subcortical regions, so a SUB-centered pattern can affect several functional domains. CA and DG, by contrast, share an ACC target in the present circuit set. Their convergence is neurobiologically plausible because medial frontal systems

participate in memory-guided action, conflict monitoring, and affective control.[29,30] The anatomical pattern alone does not establish diagnostic discrimination, however; that requires examining the sign distribution and reliability of the individual connections.

3.2. Signed evidence and alteration burden

Reliability weights ranged from 0.121 for CA–caudate to 0.185 for SUB–MTG. SUB–IFOG carried weight 0.163, CA–ACC 0.142, DG–ACC 0.134, SUB–MFG 0.130, and SUB–SMA 0.126. The modest range is important: no connection accounts for more than one fifth of the total reliability mass, so the later geometry cannot be attributed to a single overwhelmingly weighted cluster. BD had the largest alteration burden ($B = 0.879$), followed by SZ ($B = 0.689$) and MDD ($B = 0.130$). These values reflect the number and weight of supported directions, not clinical severity. In particular, MDD's low burden cannot be read as mild illness because its HAMD-17 and HAMA means were the highest among the clinical groups in Table 1.

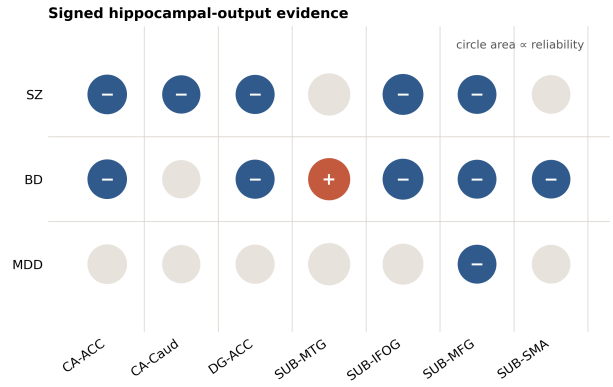

Figure 2. Signed circuit evidence.

The circle field in Fig. 2 makes three structural features visible without collapsing them into a regional list. First, SZ and BD share negative CA–ACC, DG–ACC, SUB–IFOG, and SUB–MFG entries. Second, the BD pattern contains a polarity contrast within SUB outputs: MTG is positive, whereas IFOG, MFG, and SMA are negative. Third, the MDD pattern contains only the negative SUB–MFG entry at the specified corrected threshold. Circle area varies with reliability, but direction is carried only by color and sign. The visual distinction is essential because a large common circle contributes to burden but not to entropy.

The frontal concentration fits extensive evidence that prefrontal and cingulate systems are altered across psychotic and mood syndromes.[18,19,27] Yet the pattern is more specific than a general statement about "frontal dysfunction." ACC reductions occur for both CA and DG in SZ and BD, indicating that the differentiating unit is not merely a target region; it is a target paired with a hippocampal origin. SUB–IFOG adds a lateral-orbital component, whereas SUB–MFG extends the negative sign to all three patient groups. Treating these observations as edges rather than isolated regions preserves this anatomical conditionality.

The BD-specific polarity pattern is also interpretable in relation to prior work. Middle temporal abnormalities have been reported in bipolar disorder at structural and resting-state levels,[17,34,35] while SMA coupling can vary with mood state and cortico-amygdala organization.[36,37] The present method does not label these connections as exclusive biological properties of BD. It states only that, within this corrected circuit set, they provide sign categories not assigned to the other patient groups and therefore raise BD's entropy-weighted discrimination.

3.3. Diagnostic distances and directional concordance

The smallest weighted distance was between SZ and BD ($d = 0.329$). SZ and MDD were separated by $d = 0.374$, and BD and MDD by $d = 0.433$. Signed concordance followed the complementary pattern: $C = 0.568$ for SZ–BD, $C = 0.188$ for SZ–MDD, and $C = 0.148$ for BD–MDD. Thus, the closest pair shared approximately 57% of the reliability mass altered in either group with identical direction, while concordance involving MDD was below 19%.

The pairwise quantities in Table 3 answer a question that cannot be resolved from alteration counts alone. BD has more supported entries than SZ, but the two groups are nearest because four of their negative signs coincide. MDD has only one supported entry, yet that entry matches both other groups on SUB–MFG. Its distances are therefore substantial but do not approach the theoretical maximum. The result is a compact triangle with a clear nearest pair, not three mutually opposed signatures.

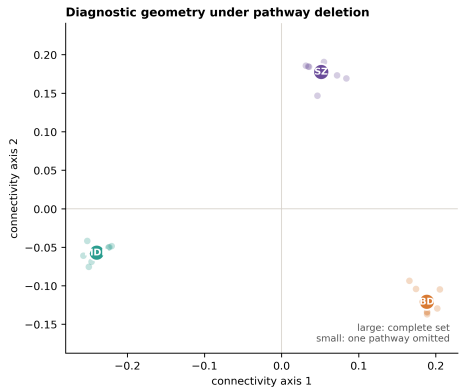

Figure 3. Diagnostic circuit geometry.

The embedding in Fig. 3 shows the complete seven-connection positions as large symbols and the seven one-pathway deletion positions as smaller symbols. SZ and BD remain adjacent under every deletion, whereas BD and MDD retain the largest separation. The small point clouds are tight relative to the intergroup triangle, indicating that the ordering is a property of the distributed

Table 3. Topological results.

Quantity	SZ–BD	SZ–MDD	BD–MDD
Weighted distance	0.329	0.374	0.433
Signed concordance	0.568	0.188	0.148
Observed total separation		1.135	
Exact-placement mean (SD)		1.282 (0.112)	
Two-sided exact probability		0.2309	
Deletion range		1.105–1.217	

sign pattern. This result matters because regional narratives often hinge on a connection described as unique. Here, no single allegedly distinctive connection is required to recover the overall diagnostic arrangement.

The proximity of SZ and BD accords with several independent biological observations. These disorders show correlated genetic risk, overlapping frontal abnormalities, and partially convergent structural phenotypes.[6,9,41] Hippocampal and ACC abnormalities have also been documented in both conditions.[31,42] The topological result is narrower than those broad literatures: within hippocampal-output circuitry, adjacency is specifically supported by concordant CA–ACC, DG–ACC, SUB–IFOG, and SUB–MFG reductions. This edge-resolved explanation is preferable to treating psychosis as a sufficient account, because the available BD group is not decomposed by psychotic history or current state.

The greater BD–MDD distance arises from both burden and polarity. BD has five negative connections and one positive connection, whereas MDD has one negative connection. SUB–MTG produces the only positive sign in the matrix and therefore contributes a full sign difference between BD and MDD. SUB–SMA, the two ACC edges, and SUB–IFOG add negative-versus-zero differences. SUB–MFG partially offsets this dispersion by providing their one concordant negative sign. In clinical terms, this arrangement suggests that affective diagnosis does not guarantee hippocampal-circuit proximity: two mood disorders can occupy distant positions when one carries a distributed psychomotor and frontotemporal pattern and the other is represented by a single common frontal connection.

The SZ–MDD distance is intermediate. SZ differs from MDD on CA–ACC, CA–caudate, DG–ACC, and SUB–IFOG, but matches it on SUB–MFG and has the same zero code on SUB–MTG and SUB–SMA. Joint zeros do not contribute to concordance, which is why $C(\mathrm{SZ}, \mathrm{MDD})$ remains low despite several visually identical empty cells. This property prevents unsupported comparisons from inflating apparent similarity and is a central advantage of the signed Jaccard definition.

3.4. Subicular dominance of diagnostic information

Entropy was zero for SUB–MFG because all patient groups had the same negative sign. Each of the remaining connections contained two sign categories and therefore contributed diagnostic information in proportion to its reliability weight. Aggregation by seed assigned 54.5% of discrimination to SUB, 30.2% to CA, and 15.4% to DG.

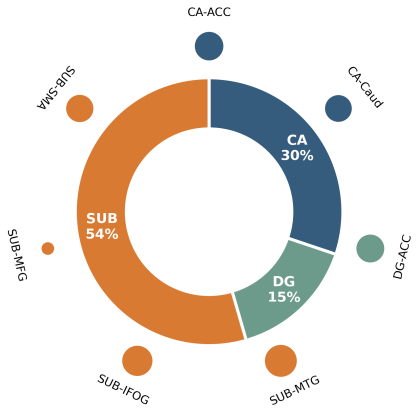

Figure 4. Seed-level discrimination.

The radial partition in Fig. 4 shows why the subicular contribution is not synonymous with uniformly strong SUB abnormality. The common SUB–MFG reduction contributes no diagnostic entropy, whereas SUB–MTG, SUB–IFOG, and SUB–SMA supply the discriminating mass. SUB dominates because it distributes differing signs across several extrahippocampal systems, not because every SUB connection is diagnostically selective. CA contributes through ACC and caudate, and DG through ACC alone.

This result supports an output-distribution account of hippocampal involvement. The subiculum is positioned to transmit hippocampal computations to diverse cortical and subcortical targets.[26] Its contribution is consequently expressed as a pattern across target systems. By contrast, CA and DG converge on ACC in the present matrix, consistent with the related roles of these subfields in associative encoding and mnemonic control.[21] The find-

ings do not imply that SUB is universally the most pathological subfield. They indicate that, among these seven corrected connections, SUB carries the largest share of between-diagnosis sign diversity.

The distinction between common abnormality and discriminating abnormality has direct implications for imaging interpretation. SUB–MFG may be valuable for understanding a cross-diagnostic process because it is negative in all patient groups, yet it cannot classify those groups by sign. SUB–MTG may be less general but more differentiating because its positive entry occurs only in BD. Studies seeking treatment targets may prioritize a consistent cross-diagnostic connection, while studies seeking mechanistic stratification may prioritize high-entropy connections. The two aims should not be conflated.

3.5. Exact placement and robustness

Observed total separation was 1.135. Across 6174 count- and polarity-preserving arrangements, the mean was 1.282 with standard deviation 0.112. The observed value lay below the mean, indicating greater compactness than a typical reassignment, but the two-sided exact probability was 0.2309 (lower-tail probability $= 0.1155$). The conditional test therefore did not establish an unusual anatomical placement at the conventional 0.05 level.

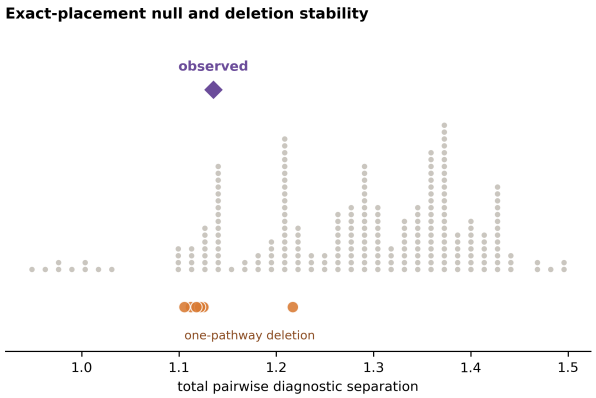

Figure 5. Placement and deletion tests.

The gray dot field in Fig. 5 displays the complete exact distribution, the purple diamond marks the observed arrangement, and the orange row shows total separation after each pathway deletion. Two conclusions follow. The geometry is descriptively compact but not conditionally exceptional, and it is stable to removal of any one connection. Deletion totals ranged only from 1.105 to 1.217, with coefficient of variation 3.4%. Uniform, F-only, cluster-only, and combined weights all retained SZ–BD as the nearest pair and BD–MDD as the farthest; total separation varied from 1.124 to 1.138 across those rules.

The non-significant exact result places an important limit on interpretation. The observed named connections produce a coherent triangle, but much of its total dispersion can be explained by the unequal numbers of supported alterations: six for BD, five for SZ, and one for MDD. Anatomical labels add interpretive content and determine which pair is nearest, yet the global amount of separation is not demonstrably rare among arrangements with the same marginal counts. Describing the matrix as a diagnostic fingerprint would therefore overstate the evidence. A more accurate conclusion is that the topology is stable and anatomically interpretable, while its global compactness remains compatible with the conditional null.

Stability under deletion provides a different and affirmative result. Exact placement evaluates whether the full arrangement is unusually dispersed or compact; deletion evaluates whether the observed ordering depends on one edge. A pattern may fail the first test and pass the second, as occurred here. This combination indicates distributed redundancy: several concordant SZ–BD reductions maintain proximity, and several BD–MDD differences maintain dispersion. The conclusion survives removal of CA–caudate, SUB–MTG, or SUB–SMA even though each has an appealing syndrome-specific interpretation.

Weight sensitivity further reduces concern that cluster extent dictates the answer. Spatial extent can be affected by smoothing and threshold choice, while F is influenced by sample size and pooled variance. The near-identical group ordering under uniform and graded weights shows that sign placement, rather than the precise reliability formula, is the principal determinant. This does not validate the signs against new data; it establishes internal robustness of the aggregate computation.

3.6. Relation to transdiagnostic neurobiology

The compact topology is compatible with contemporary transdiagnostic accounts but adds a useful qualification. Cross-disorder similarity is not uniform across the hippocampus. It is concentrated in selected hippocampal–frontal connections, while temporal, motor, and striatal connections supply diagnostic contrast. Earlier studies demonstrated cross-category alterations in local connectivity, structural networks, and frontal-posterior balance.[8,11,28] The present results show how a small circuit set can contain both adjacency and contrast without requiring a binary choice between common and diagnosis-specific pathology.

The ACC findings deserve particular attention because two hippocampal origins converge on the same target. ACC participates in cognitive control, value-guided action, and affect regulation, and it communicates with hippocampal systems involved in memory retrieval.[30] Concordant negative CA–ACC and DG–ACC signs in SZ and BD suggest that their proximity is supported by more than one hippocampal computation. Nevertheless, the current matrix cannot determine effective direction, cellular mechanism, or whether reduced resting correlation reflects impaired communication, altered common in-

put, medication exposure, or state-dependent variance.

The CA–caudate connection contributes to the SZ side of the geometry. Hippocampal-striatal coupling is relevant to associative learning, reward prediction, and dopaminergic modulation, all of which are implicated in schizophrenia.[15,32,33] Its deletion did not alter the nearest-pair ordering, so it should be regarded as a refining feature rather than the sole definition of SZ. This qualification is valuable because biologically plausible regional findings are often granted more classificatory importance than the multiconnection pattern warrants.

The SUB–IFOG connection supplies strong SZ–BD concordance. Orbitofrontal and frontoparietal systems contribute to valuation, cognitive control, and affective decision making.[29] A negative subicular-orbitofrontal relationship could therefore participate in cognitive-affective dysregulation across both disorders. Yet the absence of a corrected MDD sign in this matrix does not mean that orbitofrontal function is preserved in depression; structural and local-functional abnormalities are well documented in depressive illness.[18,19] The edge-specific claim concerns coupling with SUB under the stated procedure.

The MFG connection illustrates the opposite interpretive category. Its negative sign across all three groups makes it the sole altered connection for MDD in the matrix and a common component of SZ and BD burden. Frontal control abnormalities recur across psychiatric imaging,[4,27] and a broad hippocampal–MFG reduction is consistent with impaired coordination between memory-context systems and executive control. Because entropy is zero, however, this connection cannot explain why the patient groups occupy different positions. Biological centrality and diagnostic discrimination remain separate.

Finally, the SUB–MTG and SUB–SMA signs give BD its broadest contrast. Temporal cortex contributes to semantic, social, and affective processing, while SMA participates in internally generated action and higher-order motor control.[36] Their joint appearance may relate to the coupling of affective state with psychomotor organization in bipolar illness. The available aggregate matrix cannot test mood-state moderation, medication effects, or psychotic features, so these possibilities should motivate participant-level confirmatory work rather than be presented as resolved mechanisms.

4. CONCLUSION

The study asked whether the anatomical assignment of hippocampal-output disturbances contains diagnostic organization beyond a list of significant connections and which hippocampal sector contributes most to that organization. The answer is qualified but clear. The seven-pathway matrix forms a stable compact geometry in which schizophrenia and bipolar disorder are nearest, bipolar disorder and major depressive disorder are farthest, and the ordering persists after every single-pathway deletion and under four evidence-weighting rules. The proximity of schizophrenia and bipolar disorder is carried by concordant negative CA–ACC, DG–ACC, SUB–IFOG, and SUB–MFG signs. The greater bipolar–depression distance is carried by the distributed bipolar pattern, particularly positive SUB–MTG and negative SUB–SMA, ACC, and IFOG entries, against the single negative SUB–MFG entry assigned to depression.

The subiculum accounts for 54.5% of diagnostic discrimination because its outputs distribute sign variation across orbital frontal, temporal, and motor territories. This is not a claim that every subicular connection is selective: SUB–MFG is negative in all three patient groups and contributes burden without entropy. CA supplies 30.2% through ACC and caudate, while DG supplies 15.4% through ACC. The result therefore supports a distributed-output interpretation in which diagnostic information depends on where a hippocampal sector communicates, not merely which hippocampal label is selected.

The exact placement experiment prevents overstatement. Total separation is lower than the conditional mean but is not statistically exceptional. The observed topology is consequently compatible with alteration-count effects, even though its pairwise ordering and anatomical interpretation are robust. Hippocampal-output circuitry should not be described here as a validated diagnostic fingerprint. Its defensible role is to reveal a reproducible relation among group-level connection patterns and to identify the subicular target distribution as the main organizer of that relation.

The research question can therefore be answered directly. Disturbances of hippocampal output carry stable diagnostic geometry, but that geometry is compact rather than sharply partitioned and does not exceed the count-preserving exact expectation. Confirmation now requires participant-level connectivity estimates and independent cohorts capable of testing probabilistic direction, edge covariance, and individual transportability.

BIBLIOGRAFIA / REFERENCES

1. Song Y, Yang J, Chang M, Wei Y, Yin Z, Zhu Y, et al. Shared and distinct functional connectivity of hippocampal subregions in schizophrenia, bipolar disorder, and major depressive disorder. *Front Psychiatry*. 2022;13:993356. doi:10.3389/fpsyt.2022.993356.
2. Cuthbert BN, Insel TR. Toward the future of psychiatric diagnosis: the seven pillars of RDoC. *BMC Med*. 2013;11:126. doi:10.1186/1741-7015-11-126.
3. Insel TR, Cuthbert BN. Brain disorders? Precisely. *Science*. 2015;348:499–500. doi:10.1126/science.aab2358.
4. Goodkind M, Eickhoff SB, Oathes DJ, Jiang Y, Chang A, Jones-Hagata LB, et al. Identification of a common neurobiological substrate for mental illness. *JAMA Psychiatry*. 2015;72:305–315. doi:10.1001/jamapsychiatry.2014.2206.
5. Brainstorm Consortium, Anttila V, Bulik-Sullivan

B, Finucane HK, Walters RK, Bras J, et al. Analysis of shared heritability in common disorders of the brain. *Science*. 2018;360:eaap8757. doi:10.1126/science.aap8757.
6. Lee PH, Anttila V, Won H, Feng YCA, Rosenthal J, Zhu Z, et al. Genomic relationships, novel loci, and pleiotropic mechanisms across eight psychiatric disorders. *Cell*. 2019;179:1469–1482.e11. doi:10.1016/j.cell.2019.11.020.
7. Goldsmith DR, Rapaport MH, Miller BJ. A meta-analysis of blood cytokine network alterations in psychiatric patients: comparisons between schizophrenia, bipolar disorder and depression. *Mol Psychiatry*. 2016;21:1696–1709. doi:10.1038/mp.2016.3.
8. Wei Y, Chang M, Womer FY, Zhou Q, Yin Z, Wei S, et al. Local functional connectivity alterations in schizophrenia, bipolar disorder, and major depressive disorder. *J Affect Disord*. 2018;236:266–273. doi:10.1016/j.jad.2018.04.069.
9. Chang M, Womer FY, Edmiston EK, Bai C, Zhou Q, Jiang X, et al. Neurobiological commonalities and distinctions among three major psychiatric diagnostic categories: a structural MRI study. *Schizophr Bull*. 2018;44:65–74. doi:10.1093/schbul/sbx028.
10. Xia M, Womer FY, Chang M, Zhu Y, Zhou Q, Edmiston EK, et al. Shared and distinct functional architectures of brain networks across psychiatric disorders. *Schizophr Bull*. 2019;45:450–463. doi:10.1093/schbul/sby046.
11. Wang S, Gong G, Zhong S, Duan J, Yin Z, Chang M, et al. Neurobiological commonalities and distinctions among three major psychiatric disorders: a graph theoretical analysis of the structural connectome. *J Psychiatry Neurosci*. 2020;45:15–22. doi:10.1503/jpn.180162.
12. Duan J, Wei Y, Womer FY, Zhang X, Chang M, Zhu Y, et al. Neurobiological substrates of major psychiatric disorders: transdiagnostic associations between white matter abnormalities, neuregulin 1 and clinical manifestation. *J Psychiatry Neurosci*. 2021;46:E506–E515. doi:10.1503/jpn.200166.
13. van Erp TGM, Hibar DP, Rasmussen JM, Glahn DC, Pearlson GD, Andreassen OA, et al. Subcortical brain volume abnormalities in 2028 individuals with schizophrenia and 2540 healthy controls via the ENIGMA consortium. *Mol Psychiatry*. 2016;21:547–553. doi:10.1038/mp.2015.63.
14. Collado-Torres L, Burke EE, Peterson A, Shin J, Straub RE, Rajpurohit A, et al. Regional heterogeneity in gene expression, regulation, and coherence in the frontal cortex and hippocampus across development and schizophrenia. *Neuron*. 2019;103:203–216.e8. doi:10.1016/j.neuron.2019.05.013.
15. Lieberman JA, Girgis RR, Brucato G, Moore H, Provenzano F, Kegeles L, et al. Hippocampal dysfunction in the pathophysiology of schizophrenia: a selective review and hypothesis for early detection and intervention. *Mol Psychiatry*. 2018;23:1764–1772. doi:10.1038/mp.2017.249.
16. Hibar DP, Westlye LT, van Erp TGM, Rasmussen J, Leonardo CD, Faskowitz J, et al. Subcortical volumetric abnormalities in bipolar disorder. *Mol Psychiatry*. 2016;21:1710–1716. doi:10.1038/mp.2015.227.
17. Hibar DP, Westlye LT, Doan NT, Jahanshad N, Cheung JW, Ching CRK, et al. Cortical abnormalities in bipolar disorder: an MRI analysis of 6503 individuals from the ENIGMA Bipolar Disorder Working Group. *Mol Psychiatry*. 2018;23:932–942. doi:10.1038/mp.2017.73.
18. Chen L, Wang Y, Niu C, Zhong S, Hu H, Chen P, et al. Common and distinct abnormal frontal-limbic system structural and functional patterns in patients with major depression and bipolar disorder. *NeuroImage Clin*. 2018;20:42–50. doi:10.1016/j.nicl.2018.07.002.
19. Schmaal L, Hibar DP, Sämann PG, Hall GB, Baune BT, Jahanshad N, et al. Cortical abnormalities in adults and adolescents with major depression based on brain scans from 20 cohorts worldwide. *Mol Psychiatry*. 2017;22:900–909. doi:10.1038/mp.2016.60.
20. Amunts K, Kedo O, Kindler M, Pieperhoff P, Mohlberg H, Shah NJ, et al. Cytoarchitectonic mapping of the human amygdala, hippocampal region and entorhinal cortex: intersubject variability and probability maps. *Anat Embryol*. 2005;210:343–352. doi:10.1007/s00429-005-0025-5.
21. Yassa MA, Stark CEL. Pattern separation in the hippocampus. *Trends Neurosci*. 2011;34:515–525. doi:10.1016/j.tins.2011.06.006.
22. Haukvik UK, Tamnes CK, Söderman E, Agartz I. Neuroimaging hippocampal subfields in schizophrenia and bipolar disorder: a systematic review and meta-analysis. *J Psychiatr Res*. 2018;104:217–226. doi:10.1016/j.jpsychires.2018.08.012.
23. Hao ZY, Zhong Y, Ma ZJ, Xu HZ, Kong JY, Wu Z, et al. Abnormal resting-state functional connectivity of hippocampal subfields in patients with major depressive disorder. *BMC Psychiatry*. 2020;20:71. doi:10.1186/s12888-020-02490-7.
24. Edmiston EK, Song Y, Chang M, Yin Z, Zhou Q, Zhou Y, et al. Hippocampal resting-state functional connectivity in patients with schizophrenia and unaffected family members. *Front Psychiatry*. 2020;11:278. doi:10.3389/fpsyt.2020.00278.
25. Eklund A, Nichols TE, Knutsson H. Cluster failure: why fMRI inferences for spatial extent have inflated false-positive rates. *Proc Natl Acad Sci USA*. 2016;113:7900–7905. doi:10.1073/pnas.1602413113.
26. Matsumoto N, Kitanishi T, Mizuseki K. The subiculum: unique hippocampal hub and more. *Neurosci Res*. 2019;143:1–12. doi:10.1016/j.neures.2018.08.002.
27. Gong J, Wang J, Qiu S, Chen P, Luo Z, Wang J, et al. Common and distinct patterns of intrinsic brain activity alterations in major depression and bipolar disorder: voxel-based meta-analysis. *Transl Psychiatry*. 2020;10:353. doi:10.1038/s41398-020-01036-5.
28. Chang M, Womer FY, Gong X, Chen X, Tang L, Feng R, et al. Identifying and validating subtypes within major psychiatric disorders based on frontal-posterior

functional imbalance via deep learning. *Mol Psychiatry*. 2021;26:2991–3002. doi:10.1038/s41380-020-00892-3.
29. Menon V. Large-scale brain networks and psychopathology: a unifying triple network model. *Trends Cogn Sci*. 2011;15:483–506. doi:10.1016/j.tics.2011.08.003.
30. Rolls ET, Cheng W, Gilson M, Gong W, Deco G, Lo CZ, et al. Beyond the disconnectivity hypothesis of schizophrenia. *Cereb Cortex*. 2020;30:1213–1233. doi:10.1093/cercor/bhz161.
31. Gallinat J, McMahon K, Kühn S, Schubert F, Schaefer M. Cross-sectional study of glutamate in the anterior cingulate and hippocampus in schizophrenia. *Schizophr Bull*. 2016;42:425–433. doi:10.1093/schbul/sbv124.
32. Kraguljac NV, White DM, Hadley N, Hadley JA, Ver Hoef L, Davis E, et al. Aberrant hippocampal connectivity in unmedicated patients with schizophrenia and effects of antipsychotic medication: a longitudinal resting-state functional MRI study. *Schizophr Bull*. 2016;42:1046–1055. doi:10.1093/schbul/sbv228.
33. Sarpal DK, Robinson DG, Lencz T, Argyelan M, Ikuta T, Karlsgodt K, et al. Antipsychotic treatment and functional connectivity of the striatum in first-episode schizophrenia. *JAMA Psychiatry*. 2015;72:5–13. doi:10.1001/jamapsychiatry.2014.1734.
34. Chai X, Zhang R, Xue C, Li Z, Xiao W, Huang Q, et al. Altered patterns of the fractional amplitude of low-frequency fluctuation in drug-naive first-episode unipolar and bipolar depression. *Front Psychiatry*. 2020;11:587803. doi:10.3389/fpsyt.2020.587803.
35. Bond DJ, Su W, Honer WG, Dhanoa T, Batres YCT, Lee SS, et al. Weight gain as a predictor of frontal and temporal lobe volume loss in bipolar disorder: a prospective MRI study. *Bipolar Disord*. 2019;21:50–60. doi:10.1111/bdi.12722.
36. Nachev P, Kennard C, Husain M. Functional role of the supplementary and pre-supplementary motor areas. *Nat Rev Neurosci*. 2008;9:856–869. doi:10.1038/nrn2478.
37. Brady RO Jr, Margolis A, Masters GA, Keshavan M, Öngür D. Bipolar mood state reflected in cortico-amygdala resting-state connectivity: a cohort and longitudinal study. *J Affect Disord*. 2017;217:205–209. doi:10.1016/j.jad.2017.03.043.
38. Rubinov M, Sporns O. Complex network measures of brain connectivity: uses and interpretations. *NeuroImage*. 2010;52:1059–1069. doi:10.1016/j.neuroimage.2009.10.003.
39. Zalesky A, Fornito A, Bullmore ET. Network-based statistic: identifying differences in brain networks. *NeuroImage*. 2010;53:1197–1207. doi:10.1016/j.neuroimage.2010.06.041.
40. Smith SM, Miller KL, Salimi-Khorshidi G, Webster M, Beckmann CF, Nichols TE, et al. Network modelling methods for FMRI. *NeuroImage*. 2011;54:875–891. doi:10.1016/j.neuroimage.2010.08.063.
41. Maggioni E, Bellani M, Altamura AC, Brambilla P. Neuroanatomical voxel-based profile of schizophrenia and bipolar disorder. *Epidemiol Psychiatr Sci*. 2016;25:312–316. doi:10.1017/S2045796016000275.
42. Lim CS, Baldessarini RJ, Vieta E, Yücel M, Bora E, Sim K. Longitudinal neuroimaging and neuropsychological changes in bipolar disorder patients: review of the evidence. *Neurosci Biobehav Rev*. 2013;37:418–435. doi:10.1016/j.neubiorev.2013.01.003.